This is a preprint, the final version is subject to change, of the American Mineralogist (MSA)
Cite as Authors (Year) Title. American Mineralogist, in press.
(DOI will not work until issue is live.) DOI: http://dx.doi.org/10.2138/am-2016-5262

REVISION I

Temperature dependences of the hyperfine parameters of Fe^{2+} in $FeTiO_3$ as determined by ^{57}Fe-Mössbauer spectroscopy

Antoine Van Alboom[a] and Eddy De Grave[b]

[a] *Department of Applied Physics, University of Ghent, Valentin Vaerwyckweg 1, B-9000 Gent, Belgium,* e-mail: toon.vanalboom@ugent.be

[b] *Department of Physics and Astronomy, University of Ghent, Proeftuinstraat 86, B-9000 Gent, Belgium*

Abstract

The temperature variations of the ferrous Mössbauer parameters for a synthetic ilmenite ($FeTiO_3$) have been determined and interpreted over a very wide temperature range (5 K – 900 K). The Debye model of the lattice vibrations was used in interpreting the temperature dependence of the center shift, yielding a characteristic Mössbauer temperature of 350 ± 20 K and a zero-Kelvin intrinsic isomer shift of 1.30 ± 0.01 mm/s. The temperature dependence of the ferrous Mössbauer quadrupole splitting was interpreted using crystal field theory. A most adequate description of the experimental $\Delta E_Q(T)$ curve was obtained assuming an energy shift of at the most *ca.* 500 ± 50 cm^{-1} for the highest orbital T_{2g} level relative to the lowest level within this T_{2g} triplet. The temperature dependence of the hyperfine field was interpreted within the molecular field theory of magnetism assuming the magnetic exchange energy being a function of inter-atomic spacing, indicating a first-order magnetic transition at the magnetic-paramagnetic transition temperature of 59.0 ± 0.5 K.

This detailed presentation of Mössbauer parameters as a function of temperature can serve as a basis for easily detecting ilmenite ore at for example the lunar surface and for

monitoring by means of Mössbauer spectroscopy the reduction process of the mined mineral with the purpose of supplying a future Moon base on site with oxygen and water.

Keywords: ilmenite, Mössbauer spectroscopy, hyperfine interactions, temperature variation, Moon base

INTRODUCTION

Ilmenite ($FeTiO_3$) crystallizes in the trigonal system $R\bar{3}$, with the Fe^{2+} site being trigonally distorted (Barth and Posnjak 1934). The mineral orders antiferromagnetically below $T_N \approx 57$ K with spin direction along the *c*-axis (Grant et al. 1972, Kato et al. 1982). Mössbauer spectra (MS) for FeTiO3 have been reported earlier by, *e.g.*, Grant et al. 1972, Syono et al. 1981, Ito et al. 1982, and Nakatshuka et al. 2010. Considering the axial point symmetry of the Fe^{2+} site, Grant et al. (1972) assumed the principal axis *z* of the electric field gradient (EFG) to be parallel to *c* and hence to the direction of the hyperfine field B_{hf}. Using the typical Lorentzian- shaped six-line hyperfine pattern to fit their spectrum recorded at 5 K, the authors found values of 4.3 ± 0.3 T for the strength B_{hf} of the magnetic hyperfine field and 1.44 ± 0.01 mm/s for the quadrupole splitting constant $\frac{1}{2}e^2qQ$, with *e* the proton charge, $eq = V_{zz}$ the principal component of the EFG, and *Q* the nuclear quadrupole moment. Syono et al. (1981) measured the quadrupole splitting ΔE_Q for a synthetic $FeTiO_3$ sample at four different temperatures, i.e., 4.2, ~80, ~200, and 300 K, respectively. They observed a moderate increase in ΔE_Q from ~0.65 mm/s at 300 K to ~1.0 mm/s at ~80 K, with subsequently a relatively steep increase to 1.44 m/s at 4.2 K. They attributed the abrupt increase of ΔE_Q at low temperature to the effects of spin-orbit interaction and magnetic exchange interaction upon the electronic energy levels within the ferrous orbital T_{2g} triplet ground state. Their

theoretical considerations predicted that the drastic increase of the quadrupole splitting presumably takes place on lowering the temperature below about 25 K. Syono et al. (1981) further found for the hyperfine field B_{hf} at 4.2 K the value of 5.6 T. In a Mössbauer and neutron diffraction study of the $Co_{1-x}Fe_xO_3$ system, Ito et al. (1982) found for sample $x = 1.0$ at 4.2 K values of 4.5 ± 0.2 T for B_{hf} and 1.42 mm/s for $\frac{1}{2}e^2qQ$. They reported $\eta = 0$ for the asymmetry parameter of the EFG tensor and $\Omega = 0$ for the azimuthal angle of the direction of the hyperfine field with respect to the EFG's principal axis z. More recently, Nakatsuka et al. (2010) presented MS for a synthetic FeTiO3 powder at temperatures between room temperature (RT) and 30 K. The paramagnetic spectra clearly show the presence of ~9% Fe^{3+} cations which the authors attributed to the occurrence of inter-valence charge transfer between Fe and Ti cations. The Fe^{2+} ΔE_Q was found to be 0.64 mm/s at RT and 1.41 ± 0.08 mm/s at 30 K. The hyperfine field B_{hf} as deduced from diagonalization of the hyperfine-interaction Hamiltonian was calculated to be 4.6 ± 0.2 T.

Detailed and accurate experimental determinations of the ferrous hyperfine parameters of $FeTiO_3$ over a wide temperature range have so far not been reported. In this study, Mössbauer spectra for synthetic ilmenite, recorded at temperatures in the range from 5 K to 900 K, are presented and the temperature dependences of the various hyperfine parameters are reported. In the case of trigonal symmetry, as for $FeTiO_3$, the temperature variation of the ferrous quadrupole splitting is primarily determined by the Boltzmann population of the lower T_{2g} levels of the ferrous ^5D spectroscopic term and therefore can provide information concerning the positions and splittings of these levels. From various viewpoints within the crystal field formalism, it is attempted to extract such information about the ferrous ^5D T_{2g} levels from the presently reported experimental results for the involved ilmenite species. The temperature dependence of the hyperfine field is interpreted based on the modified molecular field model developed by Bean and Rodbell (1962), which takes into account the effects of

magnetistriction on the magnetic exchange interactions. This model may gives indications concerning the ordering of the magnetic moments.

EXPERIMENTAL

The sample material was obtained by intimately mixing Fe_2O_3 and TiO_2 powders in stoichiometric proportions. The mixture of the oxides was sintered a first time for 4 hours at 900 °C in air, and a second time again for four hours at 1000 °C and also in air. After each firing the obtained product was ball-milled for several hours with the aim of optimizing homogeneity. The final mixture was pressed into a tablet under *ca.* 2 MPa, which was sintered for 24 hours at 1200 °C in air. Subsequently, while temperature maintained at 1200 °C, a reducing gas mixture consisting of 8 % H_2 and 92 % N_2 was blown through the furnace tube during 48 hours. Powder X-ray diffraction showed that the finally obtained product was single-phase $FeTiO_3$.

Mössbauer spectra (MS) were collected in transmission geometry with the absorber plane perpendicular to the γ-ray beam. "Large-area" ^{57}Co(Rh) sources with active diameter of 5 mm and initial activity of ~75 mCi (2.78 GBq), provided by Gamma-Lab Development S.L. ©, were used. All center shift values quoted hereafter, however, are relative to α-Fe at room temperature (RT). Two different time-mode spectrometers, for low and high temperatures, respectively, each composed of Wissel GmbH© drive, detection and data-acquisition (CMCA-550) modules, were used. They operated under a triangular reference signal and were experienced to exhibit excellent linearity. The absorber thickness was approximately 10 mg Fe per cm² and counts were accumulated in 1024 channels. Asymmetry in the line intensities of the doublet spectra in the paramagnetic region was not observed, indicating that texture effects were not occurring. For all spectra the velocity (v) increment per channel, as determined from room-temperature spectra of a standard Fe foil at RT, was within the range

0.0165 ± 0.0005 mm/s. Final off-resonance counts were usually ~10^6 per channel. The temperature of the absorber was varied within the range 5 K – 300 K using the CF506 continuous flow cryostat with ITC4 temperature controller from Oxford Instruments© and using a RICOR© Mössbauer furnace, type MF-2B, for temperatures in the range 300 - 900 K equipped with in-house made temperature controller based on a chromel-alumel thermocouple.

RESULTS

Because the Fe^{2+} occupies only one crystallographic site in the ilmenite structure, it could be expected that the MS at 5 K would be adequately reproduced by one set of values for the Mössbauer parameters as assumed by Grant et al. (1972) and by Syono et al. (1981) see Table 1). However, it was observed for the presently involved $FeTiO_3$ sample that the spectra recorded at temperatures below the magnetic ordering temperature show a slight but significant line broadening, presumably attributable to the occurrence of distributions on the hyperfine parameters in particular as far as the hyperfine field B_{hf} is concerned. Therefore, MS acquired at temperatures below the transition point were numerically analyzed by model-independent hyperfine field distributions (Vandenberghe et al. 1994) using in-house developed software based on the IMSL FORTRAN library optimizer routine ZXSSQ. Because the involved parameters concern Fe^{2+} species, each of the composing elemental subcomponents was calculated by diagonalization of the full nuclear interaction Hamiltonian (Hoy and Chandra 1967). Possible distributions on the other hyperfine parameters were taken into account by assuming linear correlations between B_{hf} on the one hand and the center shift (δ), the quadrupole splitting (ΔE_Q), the zenithal angle (Ω) between the direction of B_{hf} and the axis of the principal component (V_{zz}) of the diagonalized electric field gradient tensor (EFG) and the asymmetry parameter (η) of the EFG at the other hand, respectively. As also observed

in earlier studies (Grant et al. 1972, Syono et al. 1981, Ito et al. 1982), the MS were only very weakly dependent on the azimuthal angle (Ψ) of the direction of B_{hf} with respect to the EFG axis system, and therefore in the final calculation of the MS, this angle was fixed to zero. A selection of the results (with highest probability in the respective distributions) of the parameters yielding the best agreement between calculated and experimental spectra (see Figure 1) are given in Table 1 (T = 5 K). A full list of these results is available as supplementary material.

The paramagnetic MS of the present ilmenite sample were found to be somewhat broadened, however only to an extent that can reasonably be expected for a synthetic polycrystalline oxide powder. Nevertheless, for the sake of consistency and for practical reasons, the authors preferred to numerically analyze these spectra by model-independent quadrupole splitting distributions. A possible distribution of the center shift was taken into account by imposing a linear correlation of δ with ΔE_Q. The adjusted parameter values (with highest probability in the corresponding distribution profiles) at some selected temperatures are indicated in Table 1 and for a complete list of the results at all temperatures applied in this study the reader is referred to the supplementary material. Examples of experimental and calculated spectra are reproduced in Figure 2. It is to be noted at this stage that no indication whatsoever for the presence of any significant fraction of Fe^{3+} in the structure can be noticed.

For verification, direct information about the asymmetry parameter η was also derived by analyzing a MS that was acquired at 80 K in an external magnetic field of 6 T with orientation parallel to the incident γ-rays. Satisfying agreement between the calculated and experimental spectra (see Figure 3) was obtained for the Mössbauer parameter values as reported in Table 1, with $\eta = 0.20 \pm 0.05$ and the positive sign of V_{zz}, thus being consistent with the results from the low-temperature magnetic MS. The anisotropic field-reduction quantities, occurring in the theoretical treatment of the effect of an external field acting at the

Mössbauer nuclei (Varret 1976), were calculated as *HIZ* = –1.4 T, *HIY* = –3.7 T, and *HIX* = –2.0 T (errors: ~0.3 T).

Considering the complexity of the reported Mössbauer spectra, the adjusted parameter values of the ilmenite species determined in this study are generally closely in line with those reported earlier (Grant et al. 1972, Syono et al. 1981, Ito et al. 1982, Nakatshuka et al. 2010).

DISCUSSION

Analysis of the temperature dependence of the center shift.

The temperature variation of the center shift δ is plotted in Figure 4. Generally the quantity δ consists of two contributions (De Grave and Van Alboom, 1991; Eeckhout and De Grave, 2003a). The first one is the intrinsic isomer shift (δ_I), which is determined by the s-electron density at the probe iron nuclei. In a first approximation, δ_I exhibits a slight temperature variation: $\delta_I(T) = \delta_I(0) + \alpha.10^{-5}T$ as a result of the thermal expansion of the T_{2g} and E_g wave functions of the iron probes (Perkins and Hazony 1972). The second contribution to the center shift is the second-order Doppler shift (δ_{SOD}), which arises from the non-zero squared velocity of the emitting and absorbing ^{57}Fe nuclei. Its value is strongly dependent on temperature as being related to the vibrational properties of the probe ions in the crystal structure. Within the Debye approximation for the lattice vibrational spectrum, δ_{SOD} can be calculated in terms of the so-called characteristic Mössbauer temperature, Θ_M, yielding the expression (Pound and Rebka 1960):

$$\delta_{SOD} = -\frac{9k_B\Theta_M}{16Mc}\left[1+8\left(\frac{T}{\Theta_M}\right)^4\int_0^{\frac{\Theta_M}{T}}\frac{x^3}{e^x-1}dx\right]. \quad (1)$$

where k_B and M are the Boltzmann constant and the mass of the ^{57}Fe nucleus, respectively. Θ_M is related to the well-known Debye temperature of the lattice. The values of $\delta_I(0)$, α and

Θ_M can be obtained by adjusting the theoretical expression for $\delta(T)$ to the experimental values, yielding $\delta(0)$ = 1.30 ± 0.01 mm/s, α = -1.7 ± 0.1 mm/(sK) and Θ_M = 350 ± 20 K respectively. The solid curve in Figure 4 represents the corresponding calculated temperature variation. The result for Θ_M is well in line with a general trend that Fe^{2+} Mössbauer temperatures lie between *ca*. 300 K and *ca*. 400 K, while Fe^{3+} species commonly exhibit values close to or exceeding 500 K (De Grave and Van Alboom, 1991; Eeckhout and De Grave 2003a). The value for the thermal coefficient α is close to the value that was found for triphylite, *i.e.*, -1.1 mm/(sK) (Van Alboom et al. 2011), and in absolute value somewhat lower than –6.5 mm/(sK) in eosphorite (Van Alboom et al. 2015) and –4.5 mm/(sK) obtained for hedenbergite (Eeckhout and De Grave 2003b). As has already been remarked in Van Alboom et al. (2015), generally the parameter α is ill defined because of the extremely small misfit effects it corrects for (in particular only at relatively high temperatures) and the strong interference with the parameter Θ_M in determining the goodness-of-fit of the calculated $\delta(T)$ curve. From the Mössbauer temperature, information can be extracted about the iron Mössbauer recoil-free fraction within the Debye model of the lattice vibrations (Dyar et al. 2007, 2008 and 2013).

Interpretations of the temperature dependence of the quadrupole splitting.

In Figure 5, the quadrupole splitting ΔE_Q as a function of temperature T is plotted for the presently studied ilmenite species. In their calculations concerning $\Delta E_Q(T)$, Syono et al. (1981) modeled the temperature dependence using the equivalence principle of T_{2g}- and P-states (Ballhausen 1962). Within this formalism, they found a steep increase of the quadrupole splitting at decreasing temperature below about 25 K. Contrary to this finding the presently observed increase of the quadrupole splitting with decreasing T between 120 K and 5 K is not as abrupt as observed or calculated by those authors below *ca.* 25 K. Instead, it is noticed that

193 ΔE_Q increases gradually as temperature lowers from 900 K to *ca.* 120 K, showing a
194 subsequent stronger increase in going from *ca.* 120 K to *ca.* 25 K and then reaching a
195 saturation value of ~1.44 mm/s below ~25 K (see Figure 5).

196 Generally ΔE_Q may be written as:

197 $$\Delta E_Q = \frac{1}{2} eQ|V_{zz}|\sqrt{1+\frac{\eta^2}{3}} \quad . \qquad (2)$$

198 where Q is the nuclear quadrupole moment of ^{57}Fe, e the proton charge and $\eta = \frac{V_{xx}-V_{yy}}{V_{zz}}$ the
199 asymmetry parameter of the diagonalized electric field gradient (EFG) tensor, with diagonal
200 elements V_{xx}, V_{yy} and V_{zz} ordered as $V_{zz} > V_{xx} \geq V_{yy}$. The EFG axes system is commonly
201 chosen so that $0 \leq \eta \leq 1$, thus limiting the contribution of η to the value of ΔE_Q to maximum
202 of *ca.* 15%. Therefore, ΔE_Q is mainly determined by the value of V_{zz} and much less by η. The
203 value of ΔE_Q depends on the crystallographic coordination of the Fe^{2+} ion, which is reflected
204 in the values of $V_{zz.}$ and η, both quantities being composed of a valence and a lattice
205 contribution (Van Alboom et al. 2015). In most cases, the lattice contributions are small
206 compared to the valence contributions and both have the opposite sign (Ingalls 1964).

207 The valence contributions to V_{zz} and η are determined by the Boltzmann occupation of
208 the ^5D orbital levels, the positions of which can be obtained from crystal field theory using
209 symmetry considerations dictated by the local Fe^{2+} coordination. Taking the symmetry of the
210 Fe^{2+}-site into account, therefore the splitting of the T_{2g} levels can be determined from the
211 temperature variation of ΔE_Q (Ingalls 1964).

212 Within the crystal field model, the ^5D level scheme can be obtained by diagonalization
213 of the crystal field Hamiltonian $\hat{H}_{cf}$. For trigonal symmetry $\hat{H}_{cf}$ can be expressed in the
214 equivalent operator notation (Hutchings 1964) as:

$$\hat{H}_{cf} = -\frac{2}{3}B_4\left(\hat{O}_4^0 + 20\sqrt{2}\,\hat{O}_4^3\right) + B_2^0\hat{O}_2^0 \,. \quad (3)$$

where the operators $\hat{O}_n^m$ (n = 2 and 4; m = 0 and 3) are the Stevens' equivalent operators of the related tesseral harmonics. The B coefficients depend on the charges and the relative positions of the ligands in the coordination of the Fe^{2+} probe. Spin-orbit interaction can be taken into account by adding the term $\lambda\hat{L}\hat{S}$ to the right side of Equation 3, with $\hat{L}$ and $\hat{S}$ the orbital and spin operators respectively and λ the spin-orbit interaction coefficient (Ballhausen 1962).

Due to the trigonal elongation of the Fe^{2+}-site in ilmenite and the high-spin state of the Fe^{2+}, the lower ^5D T_{2g} triplet is split into a lower doublet and a higher singlet (with orbital splitting Δ_1 relative to the doublet ground level), this being confirmed by the observed positive sign of V_{zz} (see Table 1). For trigonal symmetry, the EFG asymmetry parameter η equals zero and in a good approximation, neglecting spin-orbit effects, the valence contribution (subscript val) to ΔE_Q can then be expressed as (Ingalls 1964):

$$\Delta E_{Q,val}(T) = \Delta E_0 \frac{(2\beta^2 - \alpha^2) - \exp\left(-\frac{\Delta_1}{k_B T}\right)}{2 + \exp\left(-\frac{\Delta_1}{k_B T}\right)} \,, \quad (4)$$

where k_B is the Boltzmann constant, α and β mixing coefficients of the d_{ij} wave functions and ΔE_0 the so-called zero-Kelvin axial valence term. In Equation 4, Δ_1 is primarily determined by B_2^0 and to much less extent by B_4. The value of B_4 is directly related to the cubic splitting $10Dq$ in an octahedral crystal field ($10Dq$ = $120B_4$). Adjustment of Equation 4 to the experimental $\Delta E_Q(T)$ values for $T \geq 80$ K yields a reasonable reproduction for temperatures exceeding *ca*. 120 K (see ~~the~~ blue dashed curve in Fig. 5). However, the observed relative sharp increase of the experimental ΔE_Q values on further lowering the temperature below ~120 K is by far not predicted by the model. This finding suggests that an additional T

dependent contribution to ΔE_Q appears at low temperatures as the result of the Boltzmann occupation of intermediately lying T_{2g} energy levels resulting from a further splitting of the doublet ground level due to spin-orbit interaction.

Adding the spin-orbit term to $\hat{H}_{cf}$ in Equation 2 and adjusting B_2^0 and the spin-orbit interaction coefficient λ so that the corresponding ^5D level scheme leads to the calculated $\Delta E_Q(T)$ curve giving the best agreement with the experimental values below 300 K, yields the green fine curve in Figure 5. By this method, a more adequate accordance between calculated and experimental $\Delta E_Q(T)$ values is obtained at low temperatures. However for higher temperatures the agreement is less satisfying. From these calculations, it is concluded that the combined effect of the trigonal symmetry of the crystal field and the spin-orbit interaction alone is not sufficient to interpret the observed $\Delta E_Q(T)$ dependence fully. Also the asymmetry of the EFG cannot be understood in this case. The observation that $\eta \neq 0$ implies a deviation from axial symmetry and consequently to a further lowering of the symmetry of the Fe^{2+} coordination, thus splitting the T_{2g} triplet in three distinct orbital levels. For such a case, within crystal field theory and neglecting spin-orbit coupling, the valence contributions to the quadrupole splitting can be calculated by (Ingalls 1964):

$$\Delta E_{Q,val,zz}(T) = \Delta E_0 \frac{1-\frac{1}{2}\exp\left(-\frac{\Delta_1}{k_B T}\right)-\frac{1}{2}\exp\left(-\frac{\Delta_2}{k_B T}\right)}{1+\exp\left(-\frac{\Delta_1}{k_B T}\right)+\exp\left(-\frac{\Delta_2}{k_B T}\right)} \quad \text{and} \tag{5}$$

$$\Delta E_{Q,val,\eta}(T) = 3\,\Delta E_0 \frac{\frac{1}{2}\exp\left(-\frac{\Delta_1}{k_B T}\right)-\frac{1}{2}\exp\left(-\frac{\Delta_2}{k_B T}\right)}{1+\exp\left(-\frac{\Delta_1}{k_B T}\right)+\exp\left(-\frac{\Delta_2}{k_B T}\right)} \tag{6}$$

Taking into account that $\eta \leq 0.36$ experimentally (see Table 1), the valence contribution of η to ΔE_Q is at most only *ca.* 2.1 % (neglecting the lattice contribution to η) as can be verified from Equation 1. As such, the temperature dependence of ΔE_Q is mainly determined by the valence contribution of V_{zz}. Adjusting the theoretical $\Delta E_Q(T)$ curve using Equations 2, 5, and

6 to the experimental data finally provides an adequate agreement between the experimental and calculated $\Delta E_Q(T)$ values (see the pink bold curve in Fig. 5) and yields for the T_{2g}-splittings the values of Δ_1 = 80 ± 10 cm^{-1} and Δ_2 = 500 ± 50 cm^{-1} for the two higher orbital levels relative to the lowest level. The value of ΔE_0 was adjusted to be 1.54 ± 0.01 mm/s. Lattice contributions were adjusted to values less than 0.1 mm/s in absolute value and are therefore of minor importance. It is noted here that spin-orbit interaction also causes splitting of the orbital levels in non-degenerate sublevels, however the influence of this splitting is apparently not noticed in the observed $\Delta E_Q(T)$. The calculated values (η < 0.10) of the asymmetry parameter are small but different from zero. Within the approximations used in this approach and considering that the contribution of η values smaller than 0.36 to ΔE_Q is at the most *ca*. 2.1 % (neglecting lattice contributions – see above), one may infer that the experimental values of η are only qualitatively explained using this model. Although the asymmetry of the EFG is clear from the Mössbauer analysis, the reason of this asymmetry could not be detected nor verified by other research techniques e.g. x-ray diffraction.

Within crystal field theory, a more general theoretical treatment of the temperature dependence of ΔE_Q can be performed by a point-charge model as described earlier by Van Alboom et al. (2015). In making such calculation for the present ilmenite, using the structural data of ilmenite given by Wechsler and Prewitt (1984) and taking spin-orbit interaction into account, it was, however, not possible to reproduce the temperature dependence of ΔE_Q satisfactorily with acceptable values of the parameters appearing in the model. On the other hand, a reasonably precise description of the temperature dependence of ΔE_Q was obtained (closely following the pink curve in Fig. 5) based on an acceptable ^5D level scheme, for which the corresponding values of the model parameters seem to be unreasonable in view of theoretical values for these parameters as reported in literature (see, *e.g.,* Van Alboom et al.

2015). A possible reason for these findings can be attributed to the occurrence of covalency effects, which indeed cannot be adequately described within the crystal field model. Another reason can be found in vibronic effects as a result of orbit-lattice interactions as suggested to occur for Fe^{2+} in other trigonally distorted octahedral sites with a doublet ground state (see Eeckhout et al. 1999 and references therein).

In summary, crystal field calculations with the inclusion of a spin-orbit interaction term alone are not able to provide an acceptable interpretation of the observed $\Delta E_Q(T)$ dependence over the full temperature range applied in this work. However, the calculations as presented in this section suggest that the non-degenerate sublevels of the ^5D T_{2g} triplet are most probably spread over an energy band of ca. 500 ± 50 cm^{-1} relative to the lowest level. The creation of such a band of energy levels is believed to be due to additional effects such as, *e.g.*, spin-orbit interaction, covalency effects, vibronic coupling, etc. The Boltzmann occupation of these various levels may explain, at least qualitatively, the temperature variation of the observed $\Delta E_Q(T)$. It is plausible that, as a consequence of this occupation, ΔE_Q at first increases very gradually as temperature lowers to ca. 120 K, subsequently shows a stronger increase on further decreasing the temperature, and finally reaches a saturation value at and below *ca.* 25 K. It should be mentioned at this point that the steeper increase below ~120 K was not observed earlier and hence not predicted at all by, *e.g.,* Grant et al. (1972) or by Syono et al. (1981).

Analysis of the temperature dependence of the hyperfine field.

$FeTiO_3$ is known as a layer-type antiferromagnet (Kato et al. 1986). Following the molecular field theory of magnetism and assuming the Mössbauer magnetic hyperfine field to be proportional to the magnetization, the temperature variation of the hyperfine field, $B_{hf}(T)$, in an antiferromagnetic substance is generally reasonably described by a Brillouin curve (Morrish 1965):

$$B_{hf}(T) = B_{hf}(0) \times B_S(x) \tag{7}$$

with $B_{\mathrm{hf}}(0)$ the saturation value of the hyperfine field and $B_{\mathrm{S}}(x)$ the Brillouin function for magnetic spin moment $S = 2$ for Fe^{2+}. The argument x is given by

$$x = \frac{2T_N}{T} \frac{B_{hf}(T)}{B_{hf}(0)}. \tag{8}$$

At low temperatures, depending on the material, the magnetic moments of the magnetic ions show long range ordering, and the hyperfine field then reaches its saturation value. Due to thermal randomization, the magnetic ordering becomes more and more disturbed at increasing temperature. The Brillouin curve describes the related decrease of the hyperfine field at increasing temperature in the case of a rigid lattice for which the magnetic interaction is assumed to be independent of lattice spacing. At a certain temperature (the so-called Néel temperature T_{N}) the magnetic ordering has totally vanished and the hyperfine field becomes zero without discontinuity. Such a transformation is known to be of second order. However, this general molecular field theory has proven to be deficient in describing the observed temperature variation of the hyperfine field for many Fe^{2+}-bearing substances, including ilmenite as experienced in the present study.

A refinement of the classical general molecular field theory is provided by the model of Bean and Rodbell (1962). These authors assume that the magnetic exchange energy is a function of the inter-atomic spacing. As a consequence, a kind of thermal hysteresis in a narrow temperature range around the transition temperature is induced: the temperature at which the field becomes zero in crossing from the antiferromagnetic to the paramagnetic state, is slightly different from the temperature at which the hyperfine field becomes non-zero when temperature decreases in going from the paramagnetic to the antiferromagnetic state. Again assuming proportionality between hyperfine field and sublattice magnetization and S =

2, application of the Bean-Rodbell model to Fe^{2+} in ilmenite leads to the following expression for the argument x of the Brillouin function $B_S(x)$ in Equation 8:

$$x = \left[2 + \frac{13 b \eta_{BR}}{15} \frac{B_{hf}^2(T)}{B_{hf}^2(0)} \right] \frac{T_N}{T} \frac{B_{hf}(T)}{B_{hf}(0)} . \quad (9)$$

where the quantity η_{BR} is a measure of the departure from an ideal second-order magnetic transition. Values for η_{BR} exceeding 1 indicate first-order transitions. Values below or equal to 1 indicate second-order transitions. In the case of a rigid lattice, the value for η_{BR} equals zero and the variation of $B_{hf}(T)$ then follows the classical Brillouin curve. This theory of Bean and Rodbell predicts that, in the case of a first-order transition ($\eta_{BR} > 1$), the hyperfine field decreases less rapidly with increasing temperature as compared with the comparable rigid system. Hence, the hyperfine field will be different from zero when the Néel temperature of the comparable rigid system is reached. When temperature further increases, at a certain somewhat higher temperature the hyperfine field falls discontinuously to zero. This is demonstrated by the calculated curve in Figure 6, which adequately describes the observed variation of the hyperfine field for Fe^{2+} in the present ilmenite. The value of η_{BR} was found to be 1.56 ± 0.05, implying the magnetic transformation to be of first-order. The corresponding calculated value for T_N is 57.1 ± 0.5 K. However, as expected for a first-order transition following the model of Bean and Rodbell, the hyperfine field falls discontinuously to zero at a somewhat higher temperature, here 59.0 ± 0.5 K, as can be noticed from Figure 6. In contrary to Kato et al. (1982), the magnetic transformation of first order in the present ilmenite extends to the all temperatures $T \leq 59.0 \pm 0.5$ K. Further research is planned to confirm these results.

IMPLICATIONS

$FeTiO_3$ is a common accessory mineral in many terrestrial igneous and metamorphic rocks, and it also occurs in sedimentary deposits on earth (Bowles 2011). It is the most important source of titanium and supplies source material to the large TiO_2 pigment industry as well as to the very significant and growing titanium sponge/metal market (Choudhury et al. 2013). Ilmenite is also important for other industries, for example electronics (Raghavender et al. 2013, Yan et al. 2010), and for medical applications (Balazic et al. 2007).

Ilmenite is also an abundant component of many lunar rocks (Bowles 2011), even to that extent that it is the subject of research to extract Fe, Ti and O_2 from lunar ilmenite on the Moon itself for use in a Moon base (Schwandt et al. 2012) and to produce H_2O for human habitation by reducing lunar ilmenite (Li et al. 2012).

To make use of the ilmenite source on the Moon, knowledge about locations with a high ilmenite abundance on the lunar surface is prerequesite. In addition to high-resolution UV-VIS mapping of the lunar surface (Robinson et al. 2007), Mössbauer spectroscopy can play an important role in establishing ilmenite-rich places (Klingelhöfer 2012), because the mineral can be easily identified by its characteristic Mössbauer spectrum, which in the paramagnetic state is only determined by the center shift and the quadrupole splitting of the Fe^{2+} in its structure. Following the experiences gained on the martian surface by the Mimos II spectrometer during the Mars Exploration Rover mission of 2003, Klingelhöfer (2012) proposes to mount a Mössbauer instrument on a lunar rover, which would allow to search for ilmenite very effectively. Using Mössbauer spectroscopy in searching for locations of ilmenite-rich places on the Moon surface, the ferrous center shift and quadrupole splitting data would be of crucial importance. Also their temperature dependences will be very important parameters, because it is known that temperatures at the surface of the Moon can

change drastically, depending on where the sun is shining, ranging from about 100 degrees C at daytime to −173 degrees C at night.

Mössbauer spectroscopy could also be applied in situ to monitor the degree of reduction of ilmenite during the oxygen production process (Klingelhöfer 2012). The presented values of the Mössbauer parameters will be also very helpful in monitoring this process.

In summary, measured values of the center shift and the quadrupole splitting for ilmenite as presented in this paper therefore can be very conclusive for the identification of Lunar ilmenite and have previously never been reported over such a wide temperature range nor in such a large number of different temperatures.

Acknowledgments

This work was funded by the Fund for Scientific Research – Flanders, Belgium.

References cited

Ballhausen, C. J. (1962) Introduction to ligand field theory. McGraw-Hill Book Company, Inc., New-York.

Barth, T. F. M., and Posnjak, E. (1934) The crystal structure of ilmenite. Zeitschrift für Krystallographie, 88, 265-70.

Balazic, M., Kopac, J., Jackson, M.J., and Ahmed, W. (2007) Review: titanium and titanium alloy applications in medicine. International Journal of Nano and Biomaterials 1, 3-34.

Bean, C.P., and Rodbell D.S. (1962) Magnetic disorder as a first-order phase transformation. Physical Review, 126, 104-115.

Bowles, J.F.W. (2011) Ilmenite. In Rock-Forming Minerals: Non-Silicates: Oxides, Hydroxides and Sulphides, Eds.: Deer, Howie and Zussman, Volume 5A (Second Edition), The Geological Society of London, UK.

Choudhury, R.N.P., Pati, B., Das, P.R., Dash, R.R., and Paul, A. (2013) Development of Electronic and Electrical Materials from Indian Ilmenite. Journal of Electronic Materials, 42(4), 769-782.

De Grave, E., and Van Alboom, A. (1991) Evaluation of ferrous and ferric Mössbauer fractions. Physics and Chemistry of Minerals, 18, 337-342.

Dyar, M.D., Klima, R.L., Lindsley, D., and Pieters, C.M. (2007) Effects of differential recoil-free fraction on ordering and site occupancies in Mössbauer spectroscopy of orthopyroxenes. American Mineralogist, 92, 424-428.

Dyar, M.D., Klima, R.E., Fleagle, A., and Peel, S.E. (2013) Fundamental Mössbauer parameters of synthetic Ca-Fe-Mg pyroxenes. American Mineralogist, 98, 1172-1186.

Dyar, M.D., Schaefer, M.W., Sklute, E.C., and Bishop, J.L. (2008) Mössbauer spectroscopy of phyllosilicates: Effects of fitting models on recoil-free fractions and redox ratios. Clay Minerals, 43, 3-33.

Eeckhout, S.G., and De Grave, E. (2003a) Evaluation of ferrous and ferric Mossbauer fractions. Part II. Physics and Chemistry of Minerals, 30 (3), 142-146.

Eeckhout, S.G., and De Grave, E. (2003b) Fe-57 Mossbauer-effect studies of Ca-rich, Fe-bearing clinopyroxenes: Part I. Paramagnetic spectra of magnesian hedenbergite. American Mineralogist, 88, 1129-1137.

418 Eeckhout, S.G., De Grave, E., Vochten, R., and Blaton, N.M. (1999). Mössbauer effect study
419 of anapaite, $Ca_2Fe^{2+}(PO_4)_2.4H_2O$, and of its oxidation products. Physics and Chemistry of
420 Minerals, 26, 506-512.

421 Grant, R.W., Housley, R.M., and Geller, S. (1972) Hyperfine interactions of Fe^{2+} in ilmenite.
422 Physical Review B5, 1700-1706.

423 Hoy, G.R., and Chandra, S. (1967) Effective Field Parameters in Iron Mössbauer
424 Spectroscopy. Journal of Chemical Physics, 47, 961-965.

425 Hutchings, M.T. (1964) Point-charge calculations of energy levels of magnetic ions in
426 crystalline electric fields. Solid State Physics, 16, 227-273.

427 Ingalls, R. (1964) Electric-field gradient tensor in ferrous compounds. Physical Review,
428 133(3A), 787-795.

429 Ito, A., Morimoto, S., Someya, Y., and Ikeda, H. (1982) Mössbauer and neutron diffraction
430 studies of competing magnetic orderings in random mixtures: $Co_{1-x}Fe_xTiO_3$. Solid State
431 Communications, 41(7), 507-510.

432 Kato, H., Yamada, M., Yamauchi, H., Hiroyoshi, H., Takei, H., and Watanabe, H. (1982)
433 Metamagnetic phase transitions in $FeTiO_3$. Journal of the Physical Society of Japan, 51(6),
434 1769-1777.

435 Kato, H., Yamaguchi, Y., Yamada, M., Funahashii, S., Nakagawa, Y., and Takei, H. (1986)
436 Neutron scattering study of magnetic excitations in oblique easy-axis antiferromagnet $FeTiO_3$.
437 Journal of Physics C: Solid State Physics, 19, 6993-7011.

438 Klingelhöfer, G. (2012). Extraterrestrial Mössbauer spectroscopy. In: The Rudolf Mössbauer
439 Story. Eds.: Kalvius, M., and Kienle, P., Springer-Verlag, Berlin Heidelberg.

Li, Y., Li, X., Wang, S., Tang, H., Gan, H., Li, S., Wei, G., Zheng, Y., Tsang, K.T., and Ouyang, Z. (2012) In-Situ Water Production by Reducing Ilmenite. In: Moon: Prospective Energy and Material Resources, Ed.: Badescu, V., Springer-Verlag Berlin Heidelberg.

Morrish, A.H. (1965) The Physical Principles of Magnetism, Wiley, New-York.

Nakatsuka, D., Fujii, T., Nakanishi, M., and Takada, J. (2010) Synthesis of Ge substituted ilmenite and their magnetic and electronic properties. Journal of Physics: Conference Series 200, 012144.

Perkins, H.K., and Hazony, Y. (1972) Temperature-dependent crystal field and charge density: Mossbauer studies of FeF_2, $KFeF_3$, $FeCl_2$, and FeF_3. Physical Review B, 5, 7-18.

Pound, R.V., and Rebka, G.A.Jr. (1960) Variation with temperature of the energy of recoil free gamma rays from solids**.** Physical Review Letters, 4, 274-277.

Raghavender, A.T., Hong, N.H., Lee, K.J., Jung, M. , Skoko, Z., Cerqueira, M.F., Samantilleke, A.P., and Vasilevskiy, M. (2013) Nano-ilmenite FeTiO: Synthesis and characterization. Journal of Magnetism and Magnetic Materials 331, 129–132.

Robinson, M.S., Hapke, B.W., Garvin, J.B., Skillman, D., Bell III, J.F., Ulmer, M.P., and Pieters, C.M. (2007). High resolution mapping of TiO_2 abundances on the Moon using the Hubble Space Telescope. Geophysical Research Letters 34, L13203.

Schwandt, C., Hamilton, J.A., Fray, D.J., and Crawford, I.A. (2012) Oxygen from Lunar Regolith. In Moon: Prospective Energy and Material Resources, Ed.: Badescu, V., Springer-Verlag Berlin, Heidelberg.

Syono, Y., Ito, A., and Morimoto, S. (1981) Systematics of Mössbauer parameters in ^{57}Fe-doped titanate and germanate ilmenites. Journal of Physical Chemistry, 42, 483-486.

462 Van Alboom, A., De Grave, E., and Wohlfahrt-Mehrens, M. (2011) Temperature dependence
463 of the Fe^{2+} Mössbauer parameters in triphylite ($LiFePO_4$). American Mineralogist, 96, 408-
464 416.

465 Van Alboom, A., de Resende, V.G., da Costa, G.M., and De Grave, E. (2015) Mössbauer
466 spectroscopic study of natural eosphorite, [$(Mn,Fe)AlPO_4(OH)_2H_2O$]. American Mineralogist,
467 100, 580-587.

468 Vandenberghe, R.E., De Grave, E., and de Bakker, P.M.A. (1994) On the methodology of the
469 analysis of Mössbauer spectra. Hyperfine Interactions, 83, 29-49.

470 Varret, F. (1976) Mössbauer spectra of paramagnetic powders under applied field: Fe^{2+} in
471 fluosilicates. Journal of Physics and Chemistry of Solids, 37(3), 265-271.

472 Wechsler, B.A., and Prewitt, C.T. (1984) Crystal structure of ilmenite ($FeTiO_3$) at high
473 temperature and at high pressure. American Mineralogist, 69, 176-185.

474 Yan, S., Ge, S., Qiao, W., and Zuo, Y. (2010) Synthesis of ferromagnetic semiconductor
475 $0.67FeTiO_3$-$0.33Fe_2O_3$ powder by chemical co-precipitation. Journal of Magnetism and
476 Magnetic Materials, 322, 824–826.
477

478

479

480 **Figure captions**

481 Figure 1: Experimental (+) and calculated (full line) spectra at selected temperatures below
482 the magnetic ordering temperature (left) and corresponding B_{hf}-probability distributions
483 (right). The size of the symbols (+) roughly corresponds to twice the standard deviation (2σ)
484 for the observed counts.

485 Figure 2: Experimental (+) and calculated (full line) spectra at selected temperatures in the
486 paramagnetic region (left) and corresponding ΔE_Q -probability distributions (right). The size
487 of the symbols (+) roughly corresponds to twice the standard deviation (2σ) for the observed
488 counts.

489 Figure 3: Experimental (+) and calculated (full line) spectra at 80 K in a longitudinal external
490 magnetic field of 6 T. The size of the symbols (+) roughly corresponds to twice the standard
491 deviation (2σ) for the observed counts.

492 Figure 4: Experimental (+) and calculated (full line) center shifts as function of temperature
493 for the present ilmenite.

494 Figure 5: Experimental (+) and calculated (full lines) quadrupole splittings as function of
495 temperature for the present ilmenite. Blue dashed line: calculation in the case of trigonal
496 symmetry of the Fe^{2+}-site (adjusted for $T \geq 80$ K). Green thin line: calculation in the case of
497 trigonal symmetry of the Fe^{2+}-site and spin-orbit interaction taken into account (adjusted for T
498 $\leq$ 300 K). Pink bold line: calculation in the case of an additional distortion of the Fe^{2+}-site
499 neglecting spin-orbit interaction (adjusted for the whole T-region).

500 Figure 6: Experimental (+) and calculated (full line) hyperfine fields as function of
501 temperature in the present ilmenite, using the model of Bean and Rodbell (1962).

502

Tables

Table 1: Relevant Mössbauer parameters with highest probability in the B_{hf}- and ΔE_Q-distributions at selected temperatures for ilmenite (Γ: full width at half maximum; other symbols: see text). *: Grant et al. 1972; ⸸: Syono et al. 1981;**: measured in the present work in a longitudinal external magnetic field of 6 T. Errors for the present measurements: 1 K on T, 0.02 mm/s on δ; 0.02 mm/s on ΔE_Q; 0.05 on η; 0.1 T on B_{hf}; 2° on Ω; 0.01 mm/s on Γ.

T (K)	δ (mm/s)	ΔE_Q (mm/s)	V_{zz}	η	B_{hf}(T)	Ω (°)	Γ (mm/s)
4.2⸸		1.44		0.0	5.6	0	
5*	1.22	1.44	>0	0.0	4.3±0.3	0	
5	1.22	1.44	>0	0.29	4.5	13	0.29
80	1.19	1.00					0.26
80**	1.22	1.05	>0	0.20			0.31
295	1.07	0.65					0.26
900	0.62	0.24					0.26

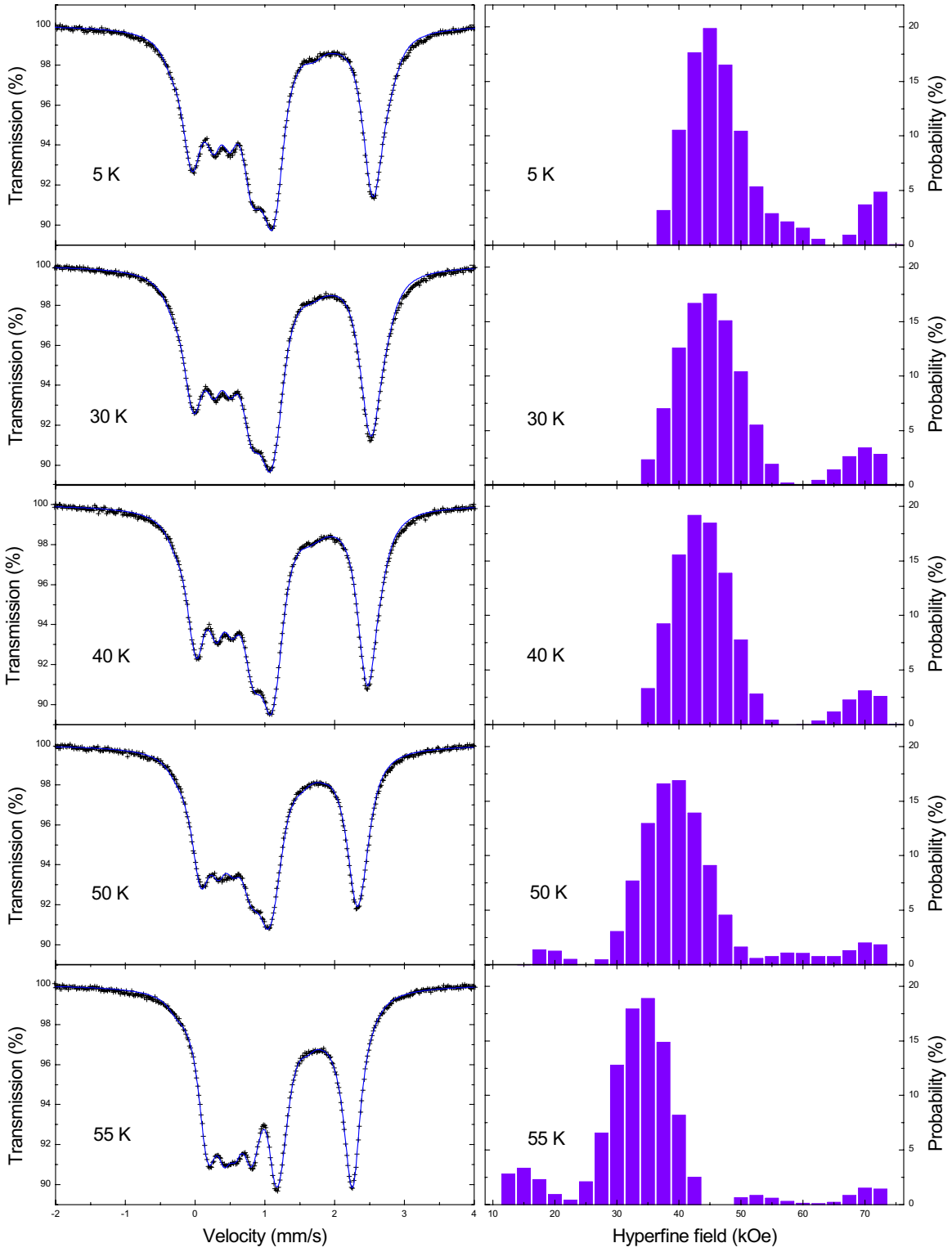
Transmission (%)
Probability (%)
5 K
30 K
40 K
50 K
55 K
Velocity (mm/s)
Hyperfine field (kOe)

Figure 1

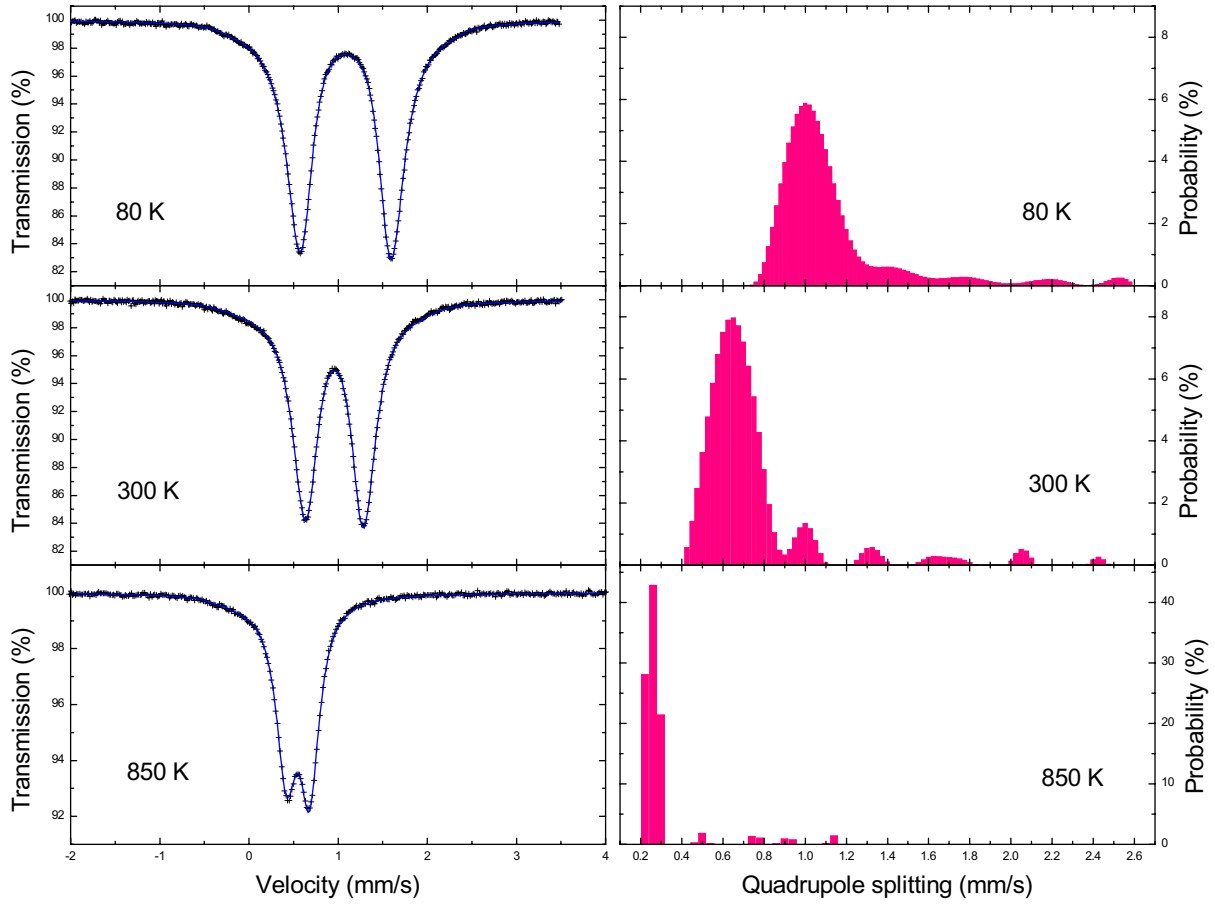
Transmission (%)
80 K
300 K
850 K
Probability (%)
Velocity (mm/s)
Quadrupole splitting (mm/s)

Figure 2

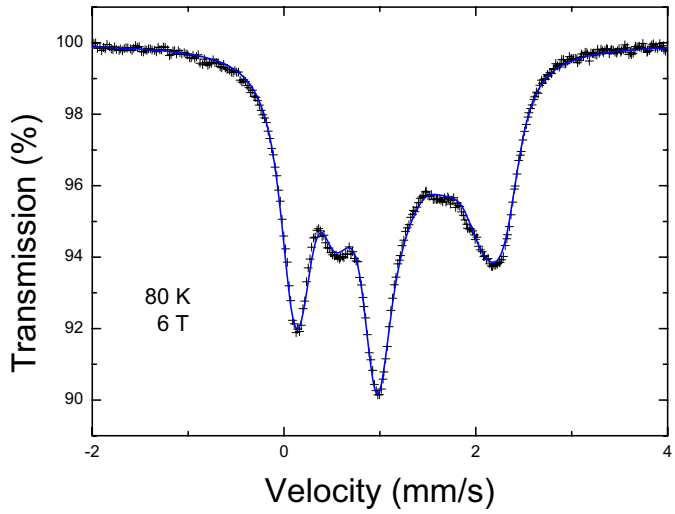

Figure 3

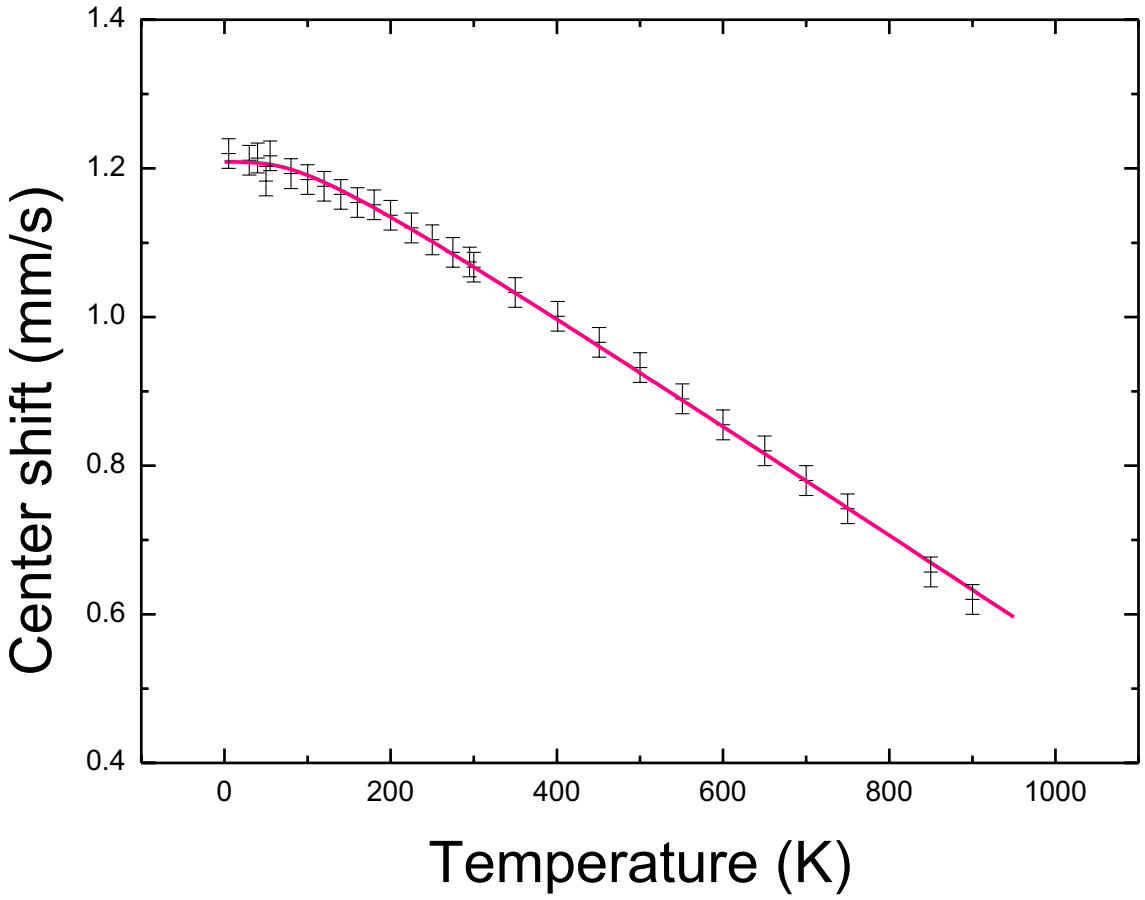
Center shift (mm/s)
1.4
1.2
1.0
0.8
0.6
0.4
0
200
400
600
800
1000
Temperature (K)

Figure 4

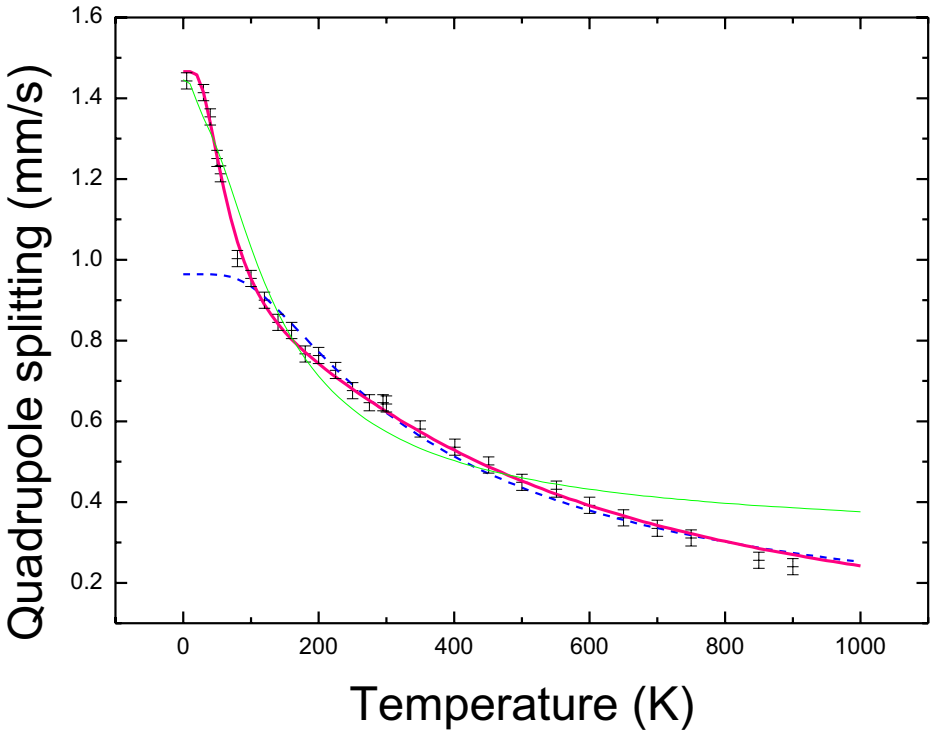
Quadrupole splitting (mm/s)
1.6
1.4
1.2
1.0
0.8
0.6
0.4
0.2
0
200
400
600
800
1000
Temperature (K)

Figure 5

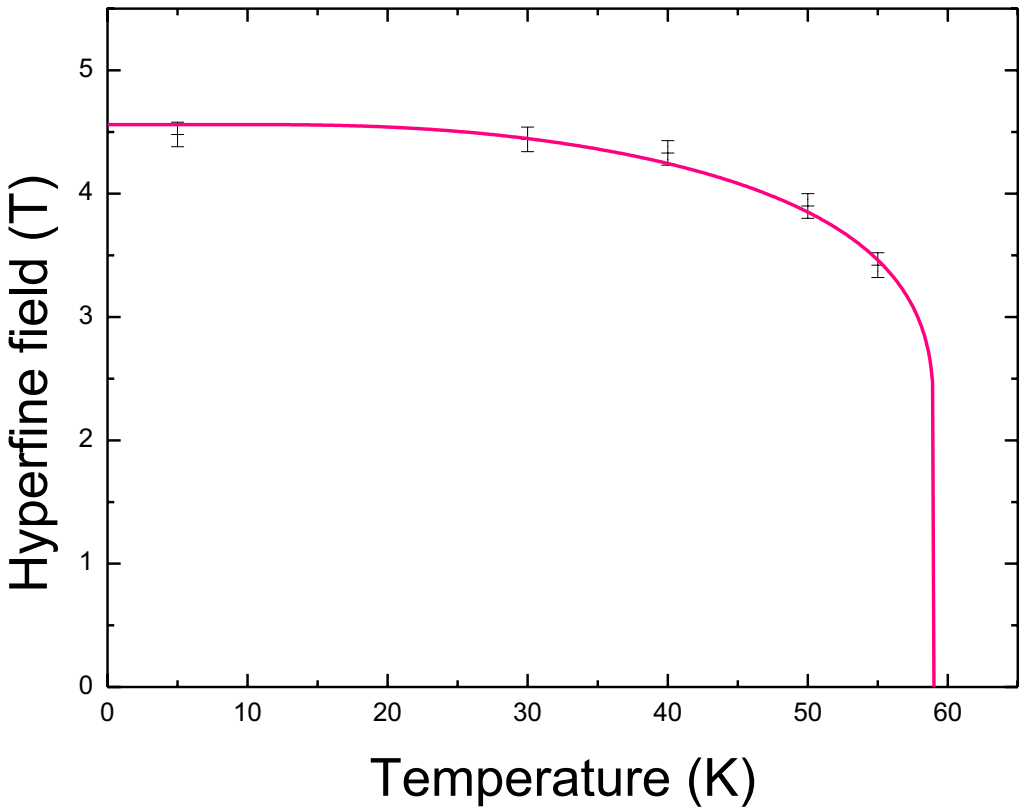

Figure 6